Ultrafast Alkaline Ni/Zn Battery Based on Ni-Foam-Supported Ni$_3$S$_2$ Nanosheets

Pu Hu,[†,‡,⊥] Tianshi Wang,[†,‡,§] Jingwen Zhao,[‡] Chuanjian Zhang,[‡] Jun Ma,[‡] Huiping Du,[‡] Xiaogang Wang,[‡] and Guanglei Cui*,[‡]

[‡]Qingdao Industrial Energy Storage Research Institute, Qingdao Institute of Bioenergy and Bioprocess Technology, Chinese Academy of Sciences, Qingdao 266101, P. R. China

[§]Institute of Materials Science and Engineering, Ocean University of China, Qingdao 266100, Shandong Province P. R. China

[⊥]University of Chinese Academy of Sciences, Beijing 100049, P. R. China

ⓈSupporting Information

ABSTRACT: Self-supported Ni$_3$S$_2$ ultrathin nanosheets were in situ formed by direct sulfurization of commercially available nickel foam using thioacetamide as sulfur source under hydrothermal process. The morphology and structure of the as-obtained sample were analyzed by using XRD, XPS, SEM, and TEM, revealing that an ultrathin nanosheets Ni$_3$S$_2$ were grown on the surface of Ni form. The as-obtained Ni$_3$S$_2$/Ni composite with uniform architecture was used as cathode material for alkaline Ni/Zn battery, which delivered high capacity of 125 mAh g^{-1} after 100 cycles with no obvious capacity fading, extraordinary rate capability (68 mAh g^{-1} at the current density of 5.0 A g^{-1}), and high operating voltage (1.75 V).

KEYWORDS: Ni/Zn battery, alkaline, cathode material, Ni$_3$S$_2$, high rate performance
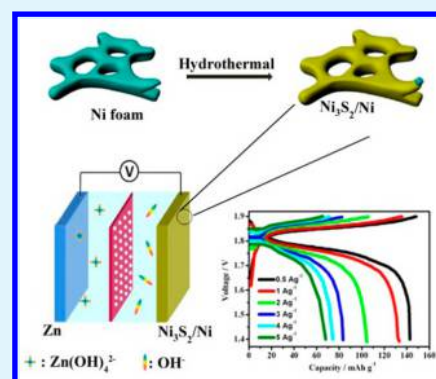
Recently, energetic multivalent ion (such as Zn^{2+}, Mg^{2+}, Al^{3+}) batteries are receiving growing attention as alternatives to dominant lithium-ion batteries for energy conversion and storage because of the limited resource of Li.[1−3] Among them, Zn-based batteries have several advantages including high energy density, low cost, nontoxicity, and so on. Especially, the aqueous electrolyte can be used, which greatly reduces the cost and ensures the safety of the batteries. These advantages make them have great competitive power in large scale application as energy storage devices.[4] The rechargeable alkaline Ni/Zn batteries present high operating voltage and capacity on the basis of the reversible electrochemical reaction between active material and OH$^-$ on cathode.[4−7]

β-Ni(OH)$_2$ are commonly used as cathode active material for conventional alkaline Ni/Zn batteries.[8,9] However, the practical application of the material is limited by the short cycling life and low energy density (ca. 70 Wh kg^{-1}).[8,10] Recently, other Ni-based compounds (such as α-Ni(OH)$_2$,[11] NiAlCo-layered double hydroxide[8] and NiO[9]) have been utilized as cathode materials aimed to improve the capacity and stability of the battery. However, poor rate property remain the main drawback because of the poor electronic conductivity and sluggish mass transfer of those materials. Therefore, novel materials and structures need to be designed to achieve the excellent kinetic property of the electrode.

Transition metal sulfides (TMSs) (such as Ni$_3$S$_2$, NiCo$_2$S$_4$, Ni$_x$Co$_{3-x}$S$_4$, etc.)[12−14] have attracted considerable attention and are extensively applied as electrode materials in Li/Na-ion batteries and supercapacitors because of their high capacity, catalytic activity, and highly reversible electrochemical process. More importantly, TMSs exhibit higher electronic conductivity than those of the oxide counterpart, which allows fast charge transfer during the Faradaic redox reactions. Especially, Ni$_3$S$_2$ delivers a high electronic conductivity of 5.5×10^4 S cm^{-1} at the ambient temperature,[15,16] being considered as an effective metallic conductor, which makes them become a promising candidate of electrode materials for fast charge transfer. Nevertheless, to the best of our knowledge, there was no attempt to utilize TMS as cathode for alkaline Zn/Ni rechargeable batteries. In alkaline solution, Ni$_3$S$_2$ exhibits high reversible electrochemical properties derived from the reversible redox of Ni(II) ↔ Ni(III) with fast Faradaic reaction between TMS and OH$^-$.

On the basis of the promising electrochemical response of Ni$_3$S$_2$ in alkaline electrolyte, in the present work, self-supported Ni$_3$S$_2$ nanosheets without any binders and additives were investigated as cathode for alkaline Zn/Ni batteries. As shown in Scheme 1, the Ni$_3$S$_2$ nanosheets were in situ grown on Ni foam substrate using thioacetamide (TAA) as sulfur source under hydrothermal process. Rechargeable Ni/Zn batteries are

Scheme 1. Schematics of the Preparation of Ni_3S_2/Ni and the Ni/Zn Battery Structure
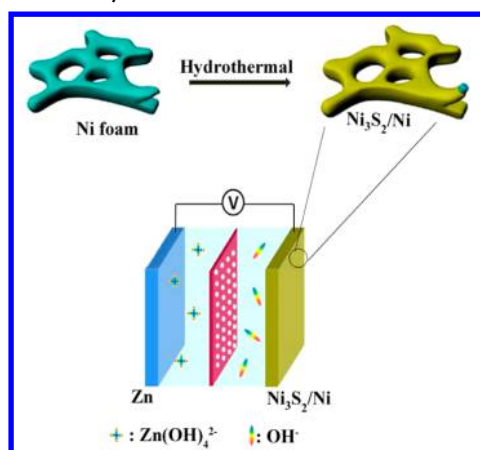
constructed by directly grown Ni_3S_2/Ni as cathode and Zn as anode in the mixture solution containing 1 M KOH and 20 mM $Zn(CH_3COO)_2$ as electrolyte. This self-supported electrode with desirable architecture is important to facilitate the mass and charge transfer during the fast electrochemical redox reaction. The reversible redox reaction of cathode and anode could be described as following

$$\text{cathode: } Ni_3S_2 + xOH^- = Ni_3S_2(OH)_x + xe^- \qquad (1)$$

$$\text{anode: } Zn(OH)_4^{2-} + 2e^- = Zn + 4OH^- \qquad (2)$$
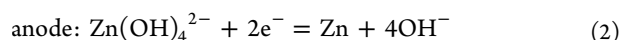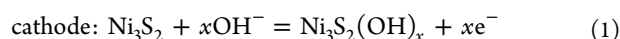
The self-supported electrode was fabricated by in situ sulfurization of commercially available Ni foam under hydrothermal condition. Figure 1a shows the typical X-ray
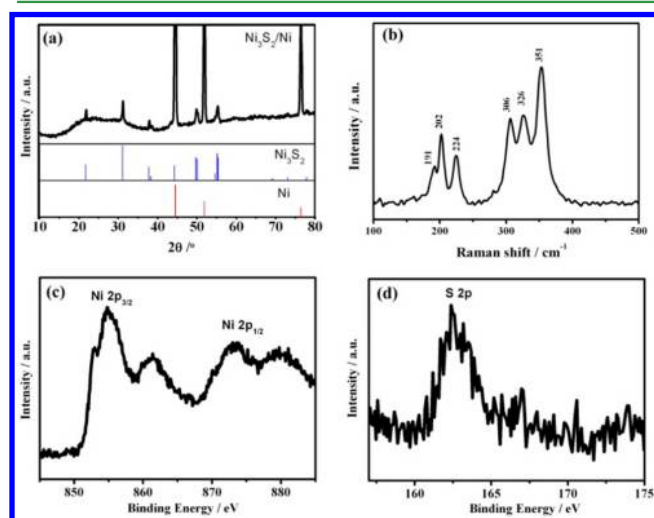
Figure 1. (a) XRD pattern; (b) Raman and (c, d) XPS spectra of the as-obtained Ni_3S_2/Ni.

diffraction(XRD) pattern of the as-obtained material, in which all the peaks can be well-indexed to the heazlewoodite-phase Ni_3S_2 with the $R32$ space group except the diffraction peaks at 44.5, 51.8, and 76.5°, corresponding to metallic Ni (JCPDS no. 65−2865). No impurity peak, such as NiS or NiS_2, was detected, implying that the surface atom of Ni foam was sulfurized to Ni_3S_2. This result suggests that the obtained material is composed of Ni_3S_2 and Ni (denoted as Ni_3S_2/Ni).

Raman and X-ray photoelectron spectroscopy (XPS) were conducted to shed more light on surface components of the as-prepared Ni_3S_2/Ni. As displayed in Figure 1b, the obvious peaks at 191, 202, 224, 306, 326, and 351 cm^{-1} of the Raman shift can be ascribed to six Raman-active modes (2A1 + 4E) of heazlewoodite-phase Ni_3S_2, in agreement with the literature reported by Cheng et al.[17] XPS spectra for Ni 2p and S 2p are shown in Figure 1c,d, respectively. The Ni 2p spectrum shows two spin−orbit doublets peaks at 855.9 (Ni $2p_{3/2}$) and 873.7 eV (Ni $2p_{1/2}$) and two corresponding satellite peaks. It could be clearly found that the peak at 852.8 eV appears near Ni $2p_{3/2}$, identical to the characteristic peak of Ni_3S_2. Binding energy of 162.5 eV in Figure 2d can be attributed to S 2p spectrum. The above data together suggest successful synthesis of Ni_3S_2/Ni composite.
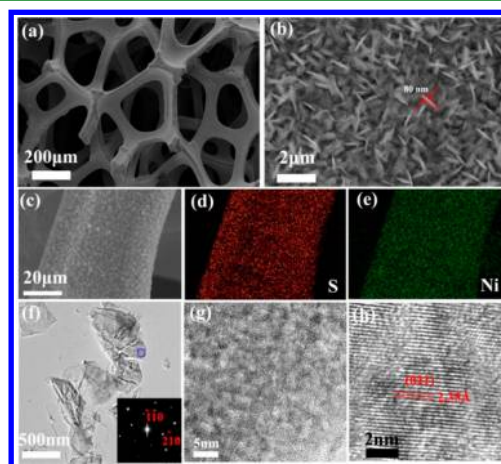

Figure 2. (a−c) Typical scanning electron microscope (SEM) images of Ni_3S_2/Ni and (d, e) elemental maps of S and Ni in Ni_3S_2/Ni; (f, g) transmission electron microscope (TEM) images and (h) high-resolution transmission electron microscope (HR-TEM) of Ni_3S_2 nanosheet.

The morphology of the Ni_3S_2/Ni maintains the 3D grid structure with hierarchical macro-porosity as the pristine Ni foam. The magnified SEM image (Figure 2b) reveals that the rippled Ni_3S_2 nanosheets with thickness of ca. 80 nm grow uniformly on the surface of Ni foam with a well-defined interconnected structure. Ni foam not only acts as the 3D skeleton to support the active material, but also provides the source of Ni for the preparation of Ni_3S_2. The energy-disperse spectroscopy (EDS) mapping clearly shows that element S distributes uniformly in the entire surface, indicative of the homogeneous growth of Ni_3S_2 (Figure 2.). The tight coupling architecture of the self-supported electrode without any additives is believed to facilitate the infiltration of electrolyte and electron transport for the fast electrochemical reaction.

TEM images (Figure 2f−h) further confirm its sheetlike morphology with micrometer scale. The dark strips are probably folded edges or wrinkles of the nanosheets. The selected-area electron diffraction (SAED) pattern shows well-defined diffraction dots, suggesting their single-crystalline characteristics. Moreover, the magnified TEM image (Figure 2g) indicates the highly porous nature of the nanosheets, which is favorable for the infiltration of electrolyte. The HRTEM image (Figure 2h) taken from the region marked by a blue rectangle in Figure 2f gives a lattice spacing of 2.35 Å, which could be indexed to the theoretical interplanar spacing of

heazlewoodite-phase Ni_3S_2 (021) planes. This is consistent with the above results of XRD and Raman spectroscopy.

The as-prepared Ni_3S_2/Ni was used as the cathode material of rechargeable alkaline Zn battery. The electrochemical performance of the $Zn-Ni_3S_2$ battery was evaluated, as shown in Figure 3. Cyclic voltammetry (CV) curves of the
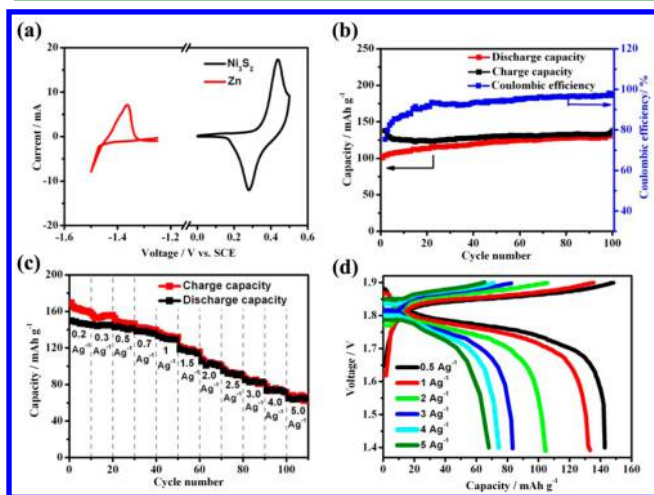
Figure 3. (a) Cyclic voltammetry of the zinc and Ni_3S_2/Ni in 1 M KOH and 20 mM $Zn(Ac)_2$ at the scan rate of 0.2 and 5 mV s^{-1}, respectively; (b) cycle performance and (c) high C-rate capacity of the battery; (d) charge−discharge curves of batteries cycling at varied current densities.

Zn and Ni_3S_2 electrodes were tested separately by using saturation calomel electrode (SCE) and Pt as reference and counter electrode in the mixed electrolyte containing 1 M KOH and 20 mM $Zn(CH_3COO)_2$. It can be clearly seen that two sets of redox peaks were observed at −1.3 to −1.5 V (vs SCE) for Zn and 0.2−0.5 V (vs SCE) for Ni_3S_2/Ni. The redox peaks at the potential of around −1.4 V (vs SCE) can be attributed to the reversible dissolution and deposition of Zn with the redox reaction of $Zn(OH)_4^{2-}/Zn$ in alkaline solution of electrolyte.[9,18] The pair of redox peaks appeared at the potential of ca. 0.3 V (vs SCE) for Ni_3S_2/Ni electrode can be attributed to the reversible redox processes of Ni^{2+}/Ni^{3+}.[19] These results could be further clarified in a three-electrode configuration using Zn as reference (Figure S2). The redox potential around 0 V (vs Zn/Zn^{2+}) demonstrates the stripping/plating of Zn. Characteristic reversible redox peaks appear at around 1.9 V, whereas no obvious peaks can be observed in that potential for pristine Ni foam, confirming that the favorable redox reaction with high reversibility was derived from active Ni_3S_2 nanosheets, as described in (eq 1), and the capacity contribution from pristine Ni foam can be negligible.

To explore the cycling performance and rate capability, the electrochemical performance of Zn battery is evaluated in the potential range of 1.4−1.9 V. As shown in Figure 3b, the electrode exhibits a high stable discharge capacity of 150 mAh g^{-1} after the initial several cycles. It maintains a capacity of 125 mAh g^{-1} after 100 cycles with no obvious capacity fading, suggesting the outstanding cycling stability. The comparison of SEM images for the Ni_3S_2/Ni electrode before cycling and after 100 cycles clearly show that the morphology of the Ni_3S_2/Ni was well-maintained, implying high stability of Ni_3S_2 in alkaline condition (Figure S3). CV curves with long-term scan show a slight negative shift of reduction potential (0.02 V) after 200

cycles, indicating again the excellent stability of Ni_3S_2/Ni electrode (as shown in Figure S4). It should be noted that the battery exhibits relatively low Coulombic efficiency of 76% in the initial cycles, which might be attributed to the onset of O_2/H_2 evolution occurring during the tail end of charge. The Coulombic efficiency increases gradually with cycling for the initial few cycles and reaches up to 92% at 20th cycle. CV curves of both Ni_3S_2/Ni and pristine Ni foam using Zn as reference and counter electrode suggest that the decomposition of H_2O with evolution of O_2 occurs at oxidative potential above 2.0 V. (Figure S2).

The high-rate capability of the battery at different current densities is displayed in Figure 3c. The reversible capacity of the battery is 148 mAh g^{-1} at the current density of 0.2 A g^{-1} and still reaches 68 mAh g^{-1} even when the current density increases to 5.0 A g^{-1}, indicating the excellent high-rate capability. Figure 3d presents the corresponding charge−discharge voltage profiles at varied current densities. At the current density of 0.5 A g^{-1}, one charge plateau and one discharge plateau at around 1.8 V with a polarization of ca. 0.1 V are observed. The separation of potential between charge−discharge plateaus slightly increases with the increasing of current density, indicating the fast electrochemical kinetics and weak polarization. This fast kinetics property can be further verified by the CV analysis. When the scan rate increases from 1 to 10 mV s^{-1}, the current enhances accordingly and the peak potential shifts only ca. 0.2 V without distortion (Figure S5a). It can be seen that the peak currents (I_p) versus square root of sweep rate ($v^{1/2}$) plots are expected to be a linear relationship (Figure S5b), indicating semi-infinite diffusion controlled kinetics of redox reaction. The extraordinary rate capability ensures the high power density of the batteries thus satisfying the application in electric vehicles.

The redox potential of Ni^{2+}/Ni^{3+} for the Ni_3S_2/Ni electrode (ca. 0.3 V vs SCE) is similar to other sulfides in alkaline condition as pseudocapacitive materials reported previously. In present study, it is noted that the discharge plateau of $Zn-Ni_3S_2/Ni$ battery is above 1.65 V at moderate current rates, which is higher than most aqueous batteries, such as $LiFePO_4/LiTi_2(PO_4)_3$ battery,[20] $Na_3V_2(PO_4)_3/NaTi_2(PO_4)_3$ battery,[21] and/or electrochemical capacitors. Although pseudocapacitors using active carbon (AC) exhibits an electrochemical activity in relatively large potential range (Figure S6), the capacity of AC is much lower than that of Zn. Moreover, the discharge potential of as-assembled AC/Ni_3S_2 electrochemical system (ca. 1.2 V) is also lower than that of the present Zn/Ni_3S_2 system (ca. 1.7 V), as shown in (Figure S7).

Although some drawbacks in terms of dendrites, corrosion and shape change of Zn electrodes need to be solved for the practical application of Ni/Zn batteries, it is believed that the combined property of the batteries can be further improved by optimization such as designing porous Zn anode and using solid-state electrolyte, and the batteries based on TMS as cathode have great potential in large scale applications of energy storage.

In summary, we have constructed an alkaline Ni/Zn battery using Ni_3S_2/Ni composite as cathode, which was fabricated by in situ sulfurization of commercially available Ni foam under hydrothermal process. The battery demonstrated excellent stability, rate capability and safety. Such advanced alkaline batteries could be a promising candidate for large-scale energy storage system. The cathode materials could be extended to

other transition metal sulfides to exploit high-performance alkaline Zn-based batteries.

■ ASSOCIATED CONTENT

Ⓢ Supporting Information

The Supporting Information is available free of charge on the ACS Publications website at DOI: 10.1021/acsami.5b09728.

> SEM images and electrochemical data. (PDF)

■ AUTHOR INFORMATION

Corresponding Author

*E-mail: cuigl@qibebt.ac.cn.Tel.: +8653280662746.

Author Contributions

†P.H. and T.W. contributed equally to this work.

Notes

The authors declare no competing financial interest.

■ ACKNOWLEDGMENTS

■ REFERENCES

(1) Gaikwad, A. M.; Whiting, G. L.; Steingart, D. A; Arias, A. C. Highly Flexible, Printed Alkaline Batteries Based on Mesh-Embedded Electrodes. *Adv. Mater.* **2011**, *23* (29), 3251−3255.

(2) Wu, N.; Yang, Z. Z.; Yao, H. R.; Yin, Y. X.; Gu, L.; Guo, Y. G. Improving The Electrochemical Performance Of The $Li_4Ti_5O_{12}$ Electrode in a Rechargeable Magnesium Battery by Lithium-Magnesium Co-intercalation. *Angew. Chem., Int. Ed.* **2015**, *54* (19), 5757−5761.

(3) Lin, M.-C.; Gong, M.; Lu, B.; Wu, Y.; Wang, D.-Y.; Guan, M.; Angell, M.; Chen, C.; Yang, J.; Hwang, B.-J.; Dai, H. An Ultrafast Rechargeable Aluminium-Ion Battery. *Nature* **2015**, *520* (7547), 325−328.

(4) Zhang, L.; Chen, L.; Zhou, X.; Liu, Z. Towards High-Voltage Aqueous Metal-Ion Batteries Beyond 1.5 V: The Zinc/Zinc Hexacyanoferrate System. *Adv. Energy Mater.* **2015**, *5* (2), 1400930.

(5) Xu, D.; Li, B.; Wei, C.; He, Y.-B.; Du, H.; Chu, X.; Qin, X.; Yang, Q.-H.; Kang, F. Preparation and Characterization of MnO_2/acid-treated CNT Nanocomposites for Energy Storage with Zinc Ions. *Electrochim. Acta* **2014**, *133*, 254−261.

(6) Alfaruqi, M. H.; Gim, J.; Kim, S.; Song, J.; Jo, J.; Kim, S.; Mathew, V.; Kim, J. Enhanced Reversible Divalent Zinc Storage in a Structurally Stable α-MnO_2 Nanorod Electrode. *J. Power Sources* **2015**, *288*, 320−327.

(7) Xu, C.; Li, B.; Du, H.; Kang, F. Energetic Zinc Ion Chemistry: The Rechargeable Zinc Ion Battery. *Angew. Chem., Int. Ed.* **2012**, *51* (4), 933−935.

(8) Gong, M.; Li, Y.; Zhang, H.; Zhang, B.; Zhou, W.; Feng, J.; Wang, H.; Liang, Y.; Fan, Z.; Liu, J.; Dai, H. Ultrafast High-Capacity NiZn Battery with NiAlCo-Layered Double Hydroxide. *Energy Environ. Sci.* **2014**, *7* (6), 2025−3032.

(9) Wang, X.; Li, M.; Wang, Y.; Chen, B.; Zhu, Y.; Wu, Y. A Zn-NiO Rechargeable Battery with Long Lifespan and High Energy Density. *J. Mater. Chem. A* **2015**, *3* (16), 8280−8283.

(10) Coates, D.; Ferreira, E.; Charkey, A. An Improved Nickel/Zinc Battery for Ventricular Assist Systems. *J. Power Sources* **1997**, *65* (1−2), 109−115.

(11) Lee, J. W.; Ahn, T.; Soundararajan, D.; Ko, J. M.; Kim, J.-D. Non-aqueous Approach to the Preparation of Reduced Graphene Oxide/α-$Ni(OH)_2$Hybrid Composites and Their High Capacitance Behavior. *Chem. Commun.* **2011**, *47* (22), 6305−6307.

(12) Zhou, W.; Cao, X.; Zeng, Z.; Shi, W.; Zhu, Y.; Yan, Q.; Liu, H.; Wang, J.; Zhang, H. One-Step Synthesis of Ni_3S_2 Nanorod@$Ni(OH)_2$ Nanosheet Core-Shell Nanostructures on a Three-Dimensional Graphene Network for High-Performance Supercapacitors. *Energy Environ. Sci.* **2013**, *6* (7), 2216−2221.

(13) Krishnamoorthy, K.; Veerasubramani, G. K.; Radhakrishnan, S.; Kim, S. J. One Pot Hydrothermal Growth of Hierarchical Nano-structured Ni_3S_2 on Ni Foam for Supercapacitor Application. *Chem. Eng. J.* **2014**, *251*, 116−122.

(14) Shen, L.; Wang, J.; Xu, G.; Li, H.; Dou, H.; Zhang, X. $NiCo_2S_4$ Nanosheets Grown on Nitrogen-Doped Carbon Foams as an Advanced Electrode for Supercapacitors. *Adv. Energy Mater.* **2015**, *5* (3), 1400977.

(15) Mi, L.; Ding, Q.; Chen, W.; Zhao, L.; Hou, H.; Liu, C.; Shen, C.; Zheng, Z. 3D Porous Nano/Micro Nickel Sulfides with Hierarchical Structure: Controlled Synthesis, Structure Characterization and Electrochemical Properties. *Dalton Trans.* **2013**, *42* (16), 5724−5730.

(16) Mi, L.; Ding, Q.; Chen, W.; Zheng, Z.; Hou, H.; Liu, C.; Shen, C. Large-Scale Stereoscopic Structured Heazlewoodite Microrod Arrays and Scale-Like Microsheets for Lithium-Ion Battery Applications. *RSC Adv.* **2012**, *2* (17), 6817−6823.

(17) Cheng, Z.; Abernathy, H.; Liu, M. Raman Spectroscopy of Nickel Sulfide Ni_3S_2. *J. Phys. Chem. C* **2007**, *111* (49), 17997−18000.

(18) Xie, X.; Yang, Z.; Feng, Z.; Zhang, Z.; Huang, J. Electrochemical Properties of ZnO Added with Zn-Al-Hydrotalcites as Anode Materials for Zinc/Nickel Alkaline Secondary Batteries. *Electrochim. Acta* **2015**, *154*, 308−314.

(19) Dai, C.-S.; Chien, P.-Y.; Lin, J.-Y.; Chou, S.-W.; Wu, W.-K.; Li, P.-H.; Wu, K.-Y.; Lin, T.-W. Hierarchically Structured Ni_3S_2/Carbon Nanotube Composites as High Performance Cathode Materials for Asymmetric Supercapacitors. *ACS Appl. Mater. Interfaces* **2013**, *5* (22), 12168−12174.

(20) Luo, J.-Y.; Cui, W.-J.; He, P.; Xia, Y.-Y. Raising the Cycling Stability of Aqueous Lithium-ion Batteries by Eliminating Oxygen in the Electrolyte. *Nat. Chem.* **2010**, *2* (9), 760−765.

(21) Park, S. I.; Gocheva, I.; Okada, S.; Yamaki, J.-I. Electrochemical Properties of NaTi2(PO4)3 Anode for Rechargeable Aqueous Sodium-Ion Batteries. *J. Electrochem. Soc.* **2011**, *158* (10), A1067−A1070.